Strong sensitivity of x-ray emission lines following charge exchange between highly charged ions and H(1*s*) in weakly screened media

N. D. Cariatore and S. Otranto
IFISUR and Departamento de Física, Universidad Nacional del Sur, 8000 Bahía Blanca, Argentina
(Received 19 August 2015; published 6 November 2015)

We use the classical trajectory Monte Carlo method to analyze charge exchange processes between fully stripped projectiles with H(1*s*) in a screened environment at impact energies in the range 18 eV/amu to 10 keV/amu. For Fe^{26+} projectiles, (*n*,*l*)-state selective charge exchange and line emission cross sections are presented for Debye screening lengths from 15 a.u. up to the unscreened case limit. At low-impact energies, a strong dependence of the hardness ratio on the Debye screening length is found. We show that such strong dependence also evidences itself for Ne^{10+}, P^{15+}, Ar^{18+}, and Kr^{36+} projectiles. Clear indications of this dependence are noticeable in the photonic spectra even for large screening lengths (∼100 a.u.).

DOI: 10.1103/PhysRevA.92.052705 PACS number(s): 34.70.+e, 32.30.Rj

I. INTRODUCTION

During the last five decades, studies of atomic collision processes such as charge exchange and ionization have not only deepened our understanding of the underlying physics, but also provided input data for radiation planning treatment codes and for magnetohydrodynamical codes designed to astrophysical environments, and paved the way for charge exchange spectroscopy regularly used in tokamak reactors for plasma diagnostics [1–4]. Actual interest is focused on refining the accuracy of these data sets and determining in which situations such refinement is particularly needed.

Hot dense plasmas, in this sense, have been the object of study for decades due to the need for interpretation of spectroscopic observations of laser-produced plasmas [5–7]. Theoretical analyses of charge exchange cross sections between ions and H(1*s*) embedded in screened media have been performed in the past decade by means of the classical trajectory Monte Carlo (CTMC) method, with particular emphasis on He^{2+} and C^{6+} projectiles [8,9], and the atomic orbital close coupling for H^+, He^{2+}, C^{6+}, and O^{8+} projectiles [10–13]. These studies revealed two main trends: (i) As the screening capability of the medium increases, the ionization process gains relevance in contrast to the charge exchange process, for which the total cross section decreases. (ii) Photonic emission following charge exchange by highly charged ions is redshifted. This is particularly noticeable for very strong screenings as has been experimentally observed in laser-produced plasmas [5,14]. The fact that the screened Coulomb potential supports a finite number of bound states leads to a termination of the line series. Hence, spectroscopic measurements of photon energies and termination frequencies can be used to gain information on the screening properties of the medium under study.

In this work, we use the classical trajectory Monte Carlo method [15–18] to study charge exchange processes involving collisions of highly charged projectiles with H(1*s*) in screened media. Our choice of hydrogen is based on considering the simplest target for which multiple-electron processes, such as multiple capture, are ruled out, allowing a more transparent analysis of the underlying physics. In particular, we focus on low-impact energies in the range 18 eV/amu to 10 keV/amu.

In Sec. II, we describe the theoretical method. In Sec. III, we show (*n*,*l*)-state selective charge exchange cross sections and the associated x-ray line emission cross sections for Fe^{26+} projectiles for different screenings. Line emission cross sections corresponding to other projectiles (Ne^{10+}, P^{15+}, Ar^{18+}, and Kr^{36+}) are also considered at this point to highlight the wide applicability of the obtained results. Finally, in Sec. IV, we present our conclusions and outlook.

II. THEORETICAL METHOD

For simplicity, the present studies are carried out using the CTMC method in its microcanonical formulation [16]. Throughout the years, this model has been widely used to explore collisions of highly charged ions with atomic hydrogen. Alternative formulations, usually denominated hydrogenic, were developed to improve the description of the initially bound electron [19,20] and are based on a discrete summation of microcanonical ensembles corresponding to different binding energies or target nuclear charges for the target electron in order to reproduce the exact quantum mechanical H(1*s*) radial distribution. Typical computational times for hydrogenic models drastically exceed those recorded for the standard microcanonical formulation and will not be used here. Throughout this work, the interaction between particles is modeled via the Debye-Hückel model,

$$V(r_{ij}) = \frac{Z_i Z_j}{r_{ij}} \exp(-r_{ij}/D), \tag{1}$$

where D is the denominated Debye screening length.

To determine the projectile (*n*,*l*) population in charge exchange processes for a given collision system, the initial and final energies for the captured electron must be quantified for the different screenings under consideration. For this task, we use Salvat's code [21]. Provided that the screening lifts the l degeneracy, for each screening considered we generate an energy $E(n,l)$ surface. For each capture event recorded and taking into account the angular momentum relative to the projectile l_c, the classical electron energy is interpolated in the

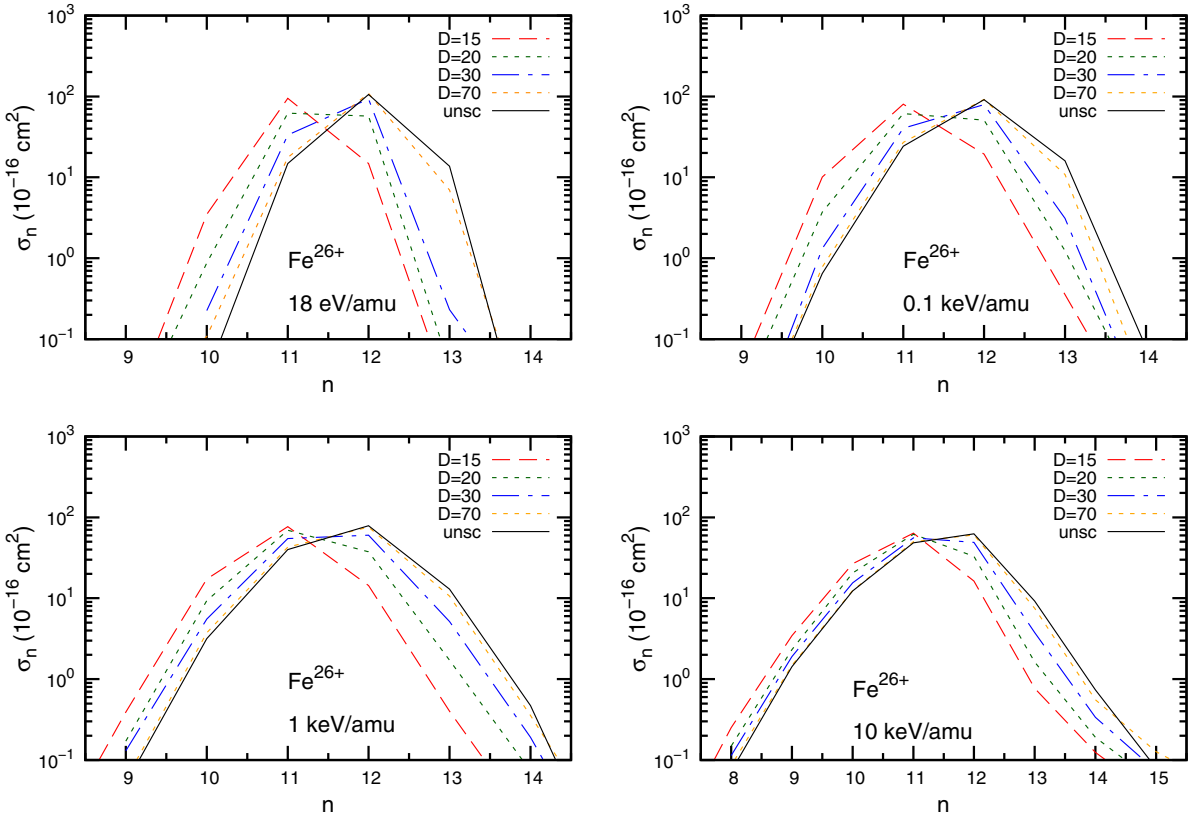

FIG. 1. (Color online) n-state selective CTMC charge exchange cross sections in $Fe^{26+} + H(1s)$ collisions at 18 eV/amu, 0.1 keV/amu, 1 keV/amu, and 10 keV/amu for different screening lengths.

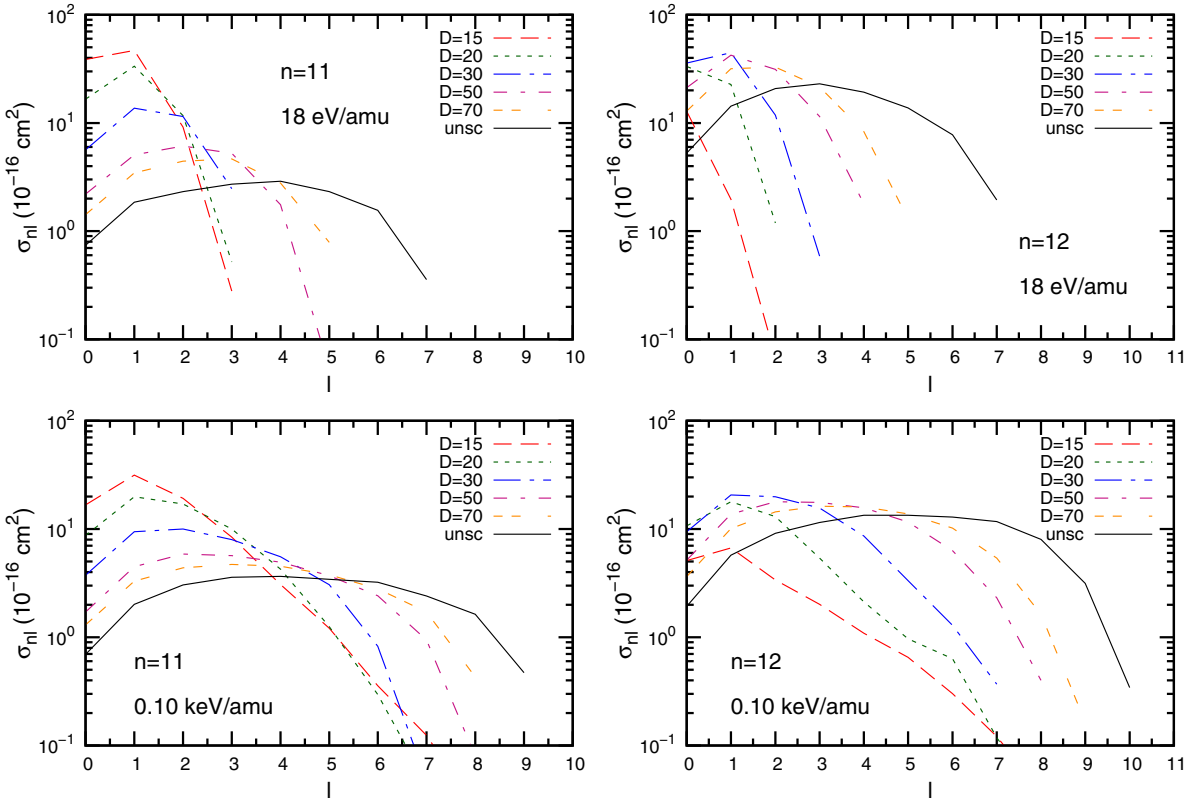

FIG. 2. (Color online) ($n = 11,l$)- and ($n = 12,l$)-state selective CTMC charge exchange cross sections in $Fe^{26+} + H(1s)$ collisions at 18 eV/amu and 0.1 keV/amu for different screening lengths.

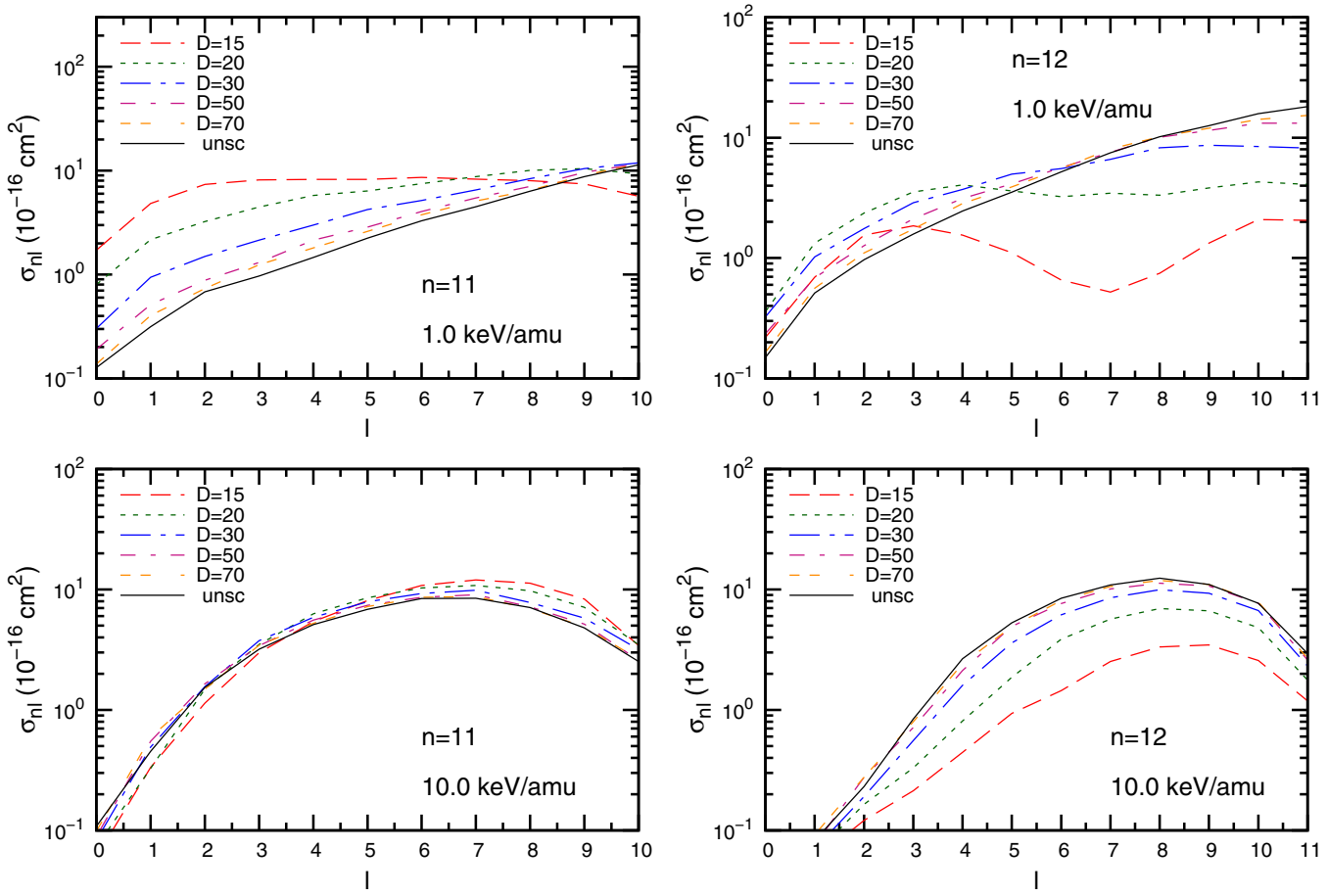

FIG. 3. (Color online) $(n = 11,l)$- and $(n = 12,l)$-state selective CTMC charge exchange cross sections in $Fe^{26+} + H(1s)$ collisions at 1 and 10 keV/amu for different screening lengths.

$E(n,l)$ surface, leading to a classical n-value n_c, which is then binned as follows to obtain the final (n,l) state:

$$n - 1/2 \leqslant n_c < n + 1/2, \tag{2}$$

$$l \leqslant (n/n_c)l_c \leqslant l + 1. \tag{3}$$

To obtain the line emission cross sections, for each D value considered, the radial wave functions obtained with Salvat's code have been used to compute cascade contributions from higher levels, branching ratios for the relevant transitions and their relative line strengths.

III. RESULTS AND DISCUSSION

In terms of the plasma electron density and temperature, the Debye length in atomic units can be expressed as [8]

$$D = 4.444\sqrt{\frac{T_e\,(\mathrm{keV})}{n_e(10^{24}\,\mathrm{cm}^{-3})}}. \tag{4}$$

In this sense, the Debye-Hückel model describes the major collective plasma effect on the interaction between charged particles provided that the coupling parameter,

$$\Gamma = 0.0232\frac{[n_e(10^{24}\,\mathrm{cm}^{-3})]^{1/3}}{T_e\,(\mathrm{keV})}, \tag{5}$$

is <1.

In what follows, we will consider screened media for which $D \geqslant 10$ a.u. This range of screening lengths pertains to environments of dense and high-temperature plasmas such as laser fusion and astrophysical plasmas of compact objects. Punctual values used in this work for the Debye screening length (in atomic units) read $D = 15,20,30,50,70,100,200,500$ and the unscreened case. At a plasma electron temperature of 1 keV, typical of laser fusion, these cases correspond to plasma electron densities of 8.78×10^{22}, 4.94×10^{22}, 2.19×10^{22}, 7.9×10^{21}, 4.0×10^{21}, 2.0×10^{21}, 4.94×10^{20}, 7.9×10^{19}, and 0 cm^{-3}, respectively. The corresponding coupling parameters are given by $\Gamma = 0.0103,0.0085,0.0065,0.0046,0.0037,$ $0.0029,0.0018,0.001$, and 0, respectively.

Another issue worth discussing before addressing our results is the denominated dynamical screening, i.e., the plasma polarization by the moving ion, which turns significant when the velocity of the ion as it moves in the plasma is comparable or larger than the thermal velocity of plasma electrons [8,22–25]. In practical terms, the dynamical screening can be

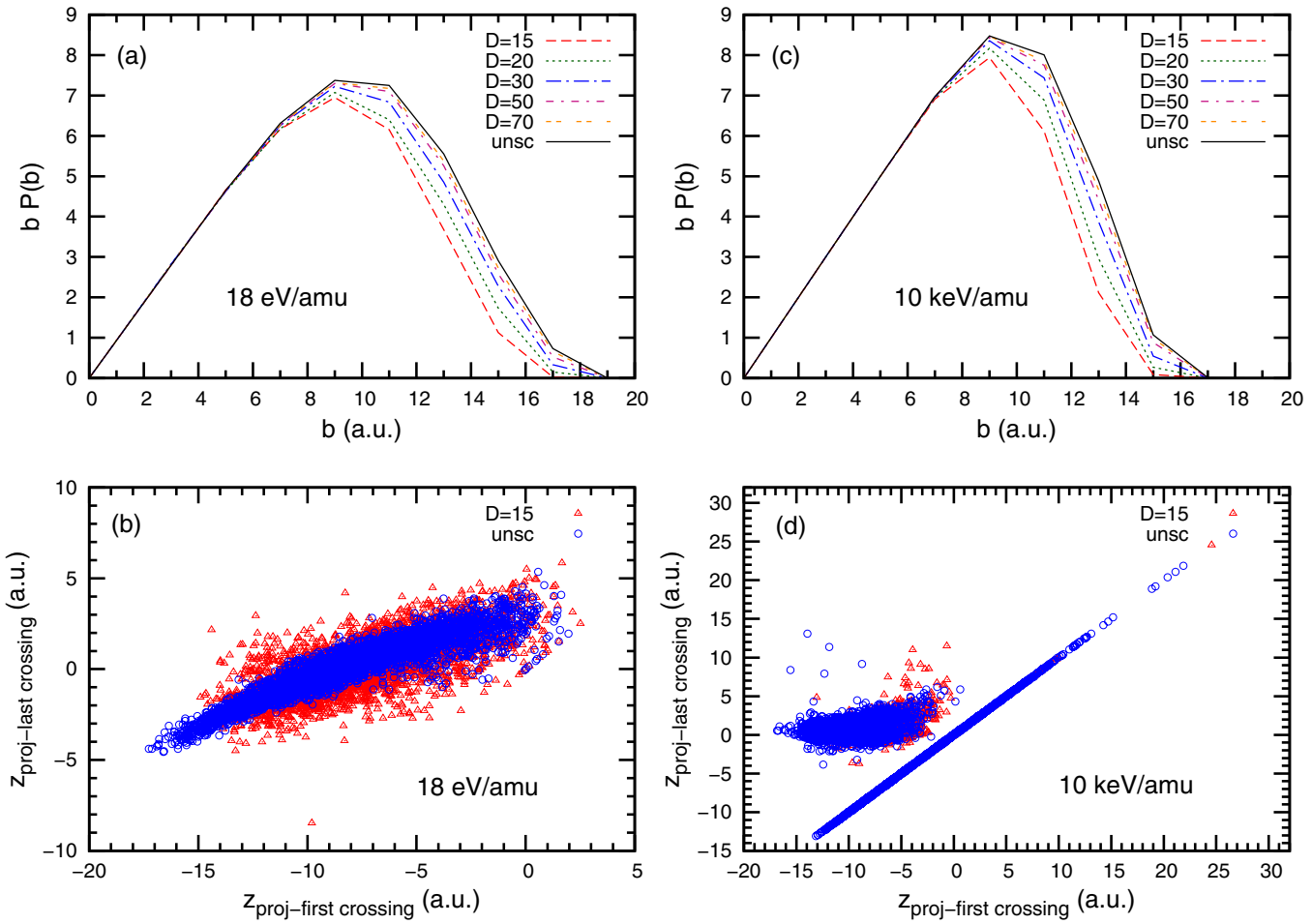

FIG. 4. (Color online) (a),(c) Charge exchange impact parameter distributions vs impact parameter b at 18 eV/amu and 10 keV/amu for different D values. (b),(d) Charge exchange events plot for the projectile position at the time the last saddle crossing occurs vs its position at the first crossing at impact energies of 18 eV/amu and 10 keV/amu, respectively. Red symbols: $D = 15$ a.u.; blue symbols: unscreened case.

included by modifying the screening length as follows:

$$D_{DS} = D\sqrt{1 + 5.54 \times 10^{-4}\frac{E\ (\mathrm{keV/amu})}{T_e\ (\mathrm{keV})}}. \qquad (6)$$

The influence of the dynamical screening, in this sense, is expected to increase as the ratio E (keV/amu)/T_e (keV) becomes larger. In that case, the screening lengths to be used to describe the interaction between the projectile and the different particles composing the target system may differ from those internally experienced by the target. Regarding charge exchange, Zhang *et al.* [8] have shown that for ion impact velocities in the order or larger than the thermal electron velocity, dynamical screening leads to a slight but progressive increase of the total cross section with respect to the one calculated with the static screening only. Provided that the largest impact energy considered in this work is 10 keV/amu, we have verified that at a plasma electron temperature of 1 keV, dynamical screening would provide a very minor correction to the static screening value D and, as a result, will not be explicitly considered in the following sections.

A. State selective electron capture in Fe^{26+} collisions on H(1s)

In Fig. 1, we show the n-state selective charge exchange cross sections for Fe^{26+} collisions on H(1s) at 18 eV/amu, 0.1 keV/amu, 1 keV/amu, and 10 keV/amu for $D =$ 15,20,30,70 a.u. and the unscreened case. While the unscreened case predicts electron capture to maximize at $n = 12$ in the whole energy range, as the medium screening increases (decreasing D values), the maximum shifts back to $n = 11$, giving a more prominent role to lower n values compared to the unscreened case. The ($n = 11$,l)- and ($n = 12$,l)-state selective charge exchange cross sections at impact energies of 18 eV/amu and 0.1 keV/amu, and 1 keV/amu and 10 keV/amu, are shown in Figs. 2 and 3, respectively. These cross sections are evaluated for the same D values explored in Fig. 1. If we first look at the unscreened (pure Coulombic) case, we note that as the impact energy decreases below 1 keV/amu, the l distributions tend to maximize at lower l values. On the other hand, at 10 keV/amu, we note that the l distribution peaks at a lower l value compared to the 1 keV/amu case, possibly indicating a less favorable matching of the initial and captured electron orbital eccentricities for the higher attainable l values [17].

Now, we focus on the changes introduced in the l distributions by considering a screened medium. As the screening increases (decreasing D values), strong deviations of the position of the maxima toward lower l values are clearly seen at the lowest-impact energies considered of 18 eV/amu and 0.1 keV/amu.

At 1 keV/amu, a strong population of lower l values compared to the unscreened case can still be seen. Moreover, while $n = 11$ shows an almost isotropical distribution for $D = 15$ a.u., for $n = 12$ an oscillatory behavior can be seen, highlighting how as the impact energy increases the larger l values become more relevant. Finally, at 10 keV/amu, the l distributions for the screened cases now maximize in larger l values, which, as D decreases, tend to slightly shift forward compared to the unscreened case.

In order to gain insight into the physics behind the strong changes seen in the l distributions, especially at low-impact energies, we now check if the reaction volume in which the charge exchange process takes place is somehow affected by the screening. Two quantities are evaluated for this task: the distribution of impact parameters relevant for charge exchange and the range of projectile z-coordinate values (coordinate along the beam axis) in which the charge exchange reaction takes place. In practice, we define this region by identifying the first and last crossing of the potential saddle by the electron [26,27]. These quantities are, respectively, shown in Figs. 4(a) and 4(b) at an impact energy of 18 eV/amu, and Figs. 4(c) and 4(d) at 10 keV/amu. In Figs. 4(a) and 4(c), we observe that as D decreases, the b distribution shrinks. However, changes are so minor that we can safely consider that the range of impact parameters relevant for charge exchange is almost the same in all cases explored. This is possibly a consequence of the fact that as the potential range decreases, so does the binding energy of the target, providing a balancing counter effect on the physical dimensions relevant to charge exchange. Figures 4(b) and 4(d), on the other hand, show that the projectile z range relevant for charge exchange is almost the same if one considers either our strongest screening $D = 15$ a.u. or the unscreened case. It is worth noting that while at 18 eV/amu, we have identified up to 69 saddle crossings, at 10 keV/amu, the one- and three-crossings mechanisms provide 99% of the charge exchange events. Together, these results show that the reaction volume remains the same for the screenings considered throughout this work.

A different perspective is explored in Figs. 5(a) and 5(b), in which we show an events plot of the final electron l value in the projectile reference frame plotted vs the l value that the same electron had at its last saddle crossing, at impact energies of 18 eV/amu and 10 keV/amu, respectively. As in the previous figure, we compare the unscreened case results to those corresponding to the maximum screening considered here ($D = 15$ a.u.). Major changes are now seen and help us identify the underlying physical mechanism. As the captured electron recedes with the projectile, after crossing the potential saddle for the last time, it keeps on feeling the pull of the recoil ion in a postcollisional stage. This attractive force modifies the l value of the electron, which otherwise would remain constant provided that the force exerted by the projectile is of a central nature. The postcollisional interaction picture is expected to gain relevance as the impact energy decreases in concordance with the results shown in Figs. 5(a) and 5(b).

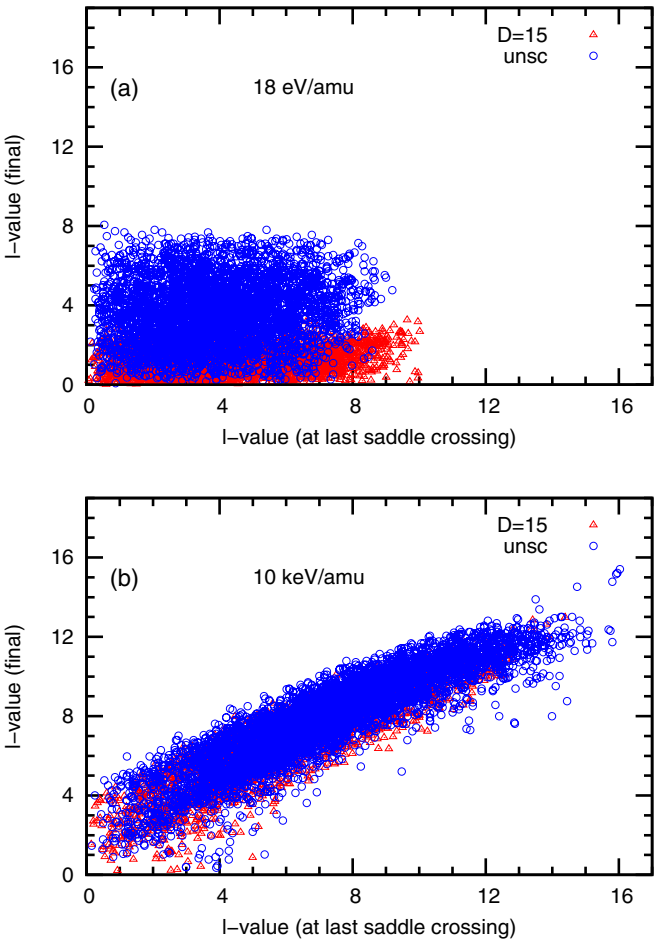

FIG. 5. (Color online) Events plot of the final l value in the projectile reference frame vs the l value at its last saddle crossing. (a) 18 eV/amu, (b) 10 keV/amu. Red symbols: $D = 15$ a.u.; blue symbols: unscreened case.

In the next section, we analyze how this situation reflects on the line emission cross sections.

B. Line emission cross sections

In Fig. 6, we show the x-ray line emission cross sections representing the Lyman transitions $np \rightarrow 1s$ following charge exchange of Fe^{26+} with H($1s$) at 18 eV/amu, 0.1 keV/amu, 1 keV/amu, and 10 keV/amu for $D = 15,30,50,70,100$ a.u. and the unscreened case.

Lyman lines are convoluted by means of Gaussian functions with an energy resolution of 250 eV FWHM, typical of Ge detectors actually under use in many laboratories worldwide. Moreover, to help visualize the differences, all curves have been normalized to the $D = 15$ a.u. case at the Lyman-α peak. Drastic differences are seen for the relative intensity of the higher Lyman lines compared to the Lyman-α line at impact energies below 1 keV/amu. These results are in concordance with the l distributions analyzed in the previous section and are evident even for very weak screenings ($D \sim 100$ a.u.) at the lowest energy considered in this work.

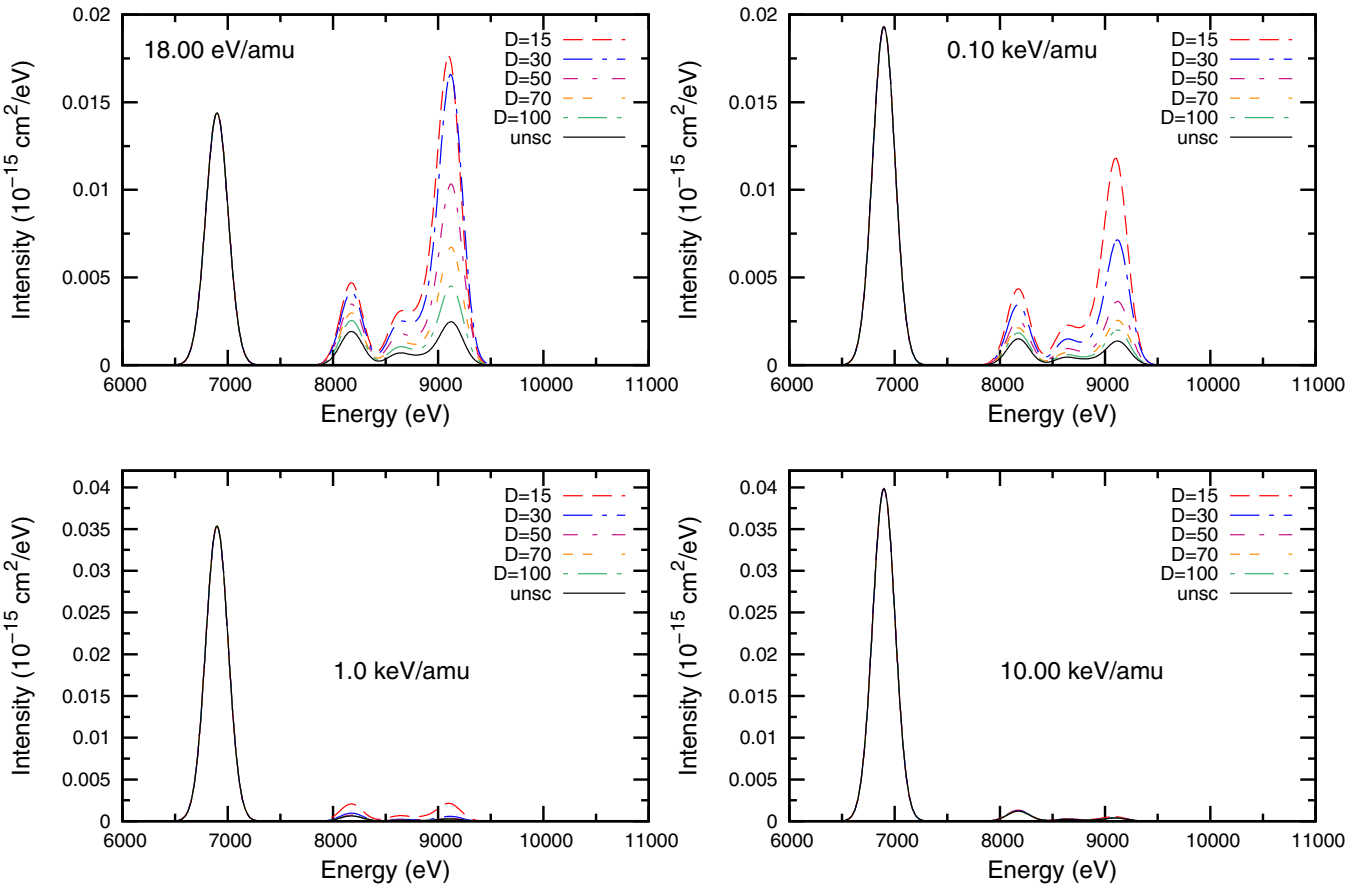

FIG. 6. (Color online) X-ray line emission cross sections following charge exchange Fe^{26+} collisions with H(1s) at 18 eV/amu, 0.1 keV/amu, 1 keV/amu, and 10 keV/amu. Results obtained for different D values are explicitly shown. The cross sections have been normalized to the $D = 15$ a.u. case at the Lyman-α peak.

In Fig. 7, we show the "hardness ratio" R, which is defined as the line emission cross section for the $np \rightarrow 1s$ transition, $n > 2$, divided by that for the Lyman-α ($2p \rightarrow 1s$ transition) value, at the lowest-impact energy considered of 18 eV/amu. This parameter allows a fast indirect inspection of the l distribution. Other projectiles (Ne^{10+}, P^{15+}, Ar^{18+}, and Kr^{36+}) are explicitly considered at this point to highlight

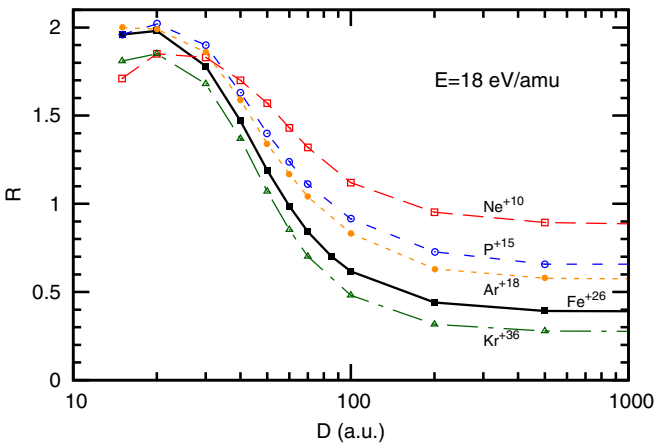

FIG. 7. (Color online) Hardness ratio R as a function of the screening length D for highly charged ions collisions on H(1s) at 18 eV/amu.

the validity of the results so far discussed for Fe^{26+} to other collision systems involving highly charged projectiles. In all cases, a strong dependence of R on the D value can be clearly observed, leading to increasing values of R as the screening length decreases. These results clearly indicate that similar trends to those presented for Fe^{26+} can be expected for the l distributions corresponding to any of these highly charged projectiles. Moreover, present CTMC results suggest that spectra will reflect the fact that the collision system is embedded in a screening medium, even for screening lengths for which the redshift of the emission lines would lay well within the resolution achieved with state-of-the-art spectrometers.

IV. CONCLUSIONS

In this work, we have studied the charge exchange process between highly charged ions and H(1s) embedded in a weakly screened medium at a state selective level. In particular, we have used Fe^{26+} as a projectile to develop our (n,l)-state selective analyses.

We have found that as the screening of the medium increases, the n distributions shift their maxima to lower values. In addition, at low-impact energies, the l distributions show a noticeable shift of their peaks to lower l values. This shift increases for decreasing screening lengths.

Present results suggest that the reaction volume is almost the same for all cases hereby considered and the drastic change in the l distributions is due to differences in the postcollisional interactions among particles under screened media. X-ray line emission cross sections also show these effects, which, besides changes in the absolute magnitudes of the Lyman lines, turn evident by increasing the relative intensity of the higher Lyman lines compared to the Ly-α line. Such differences in the spectra are especially noticeable at low-impact energies even for screening lengths in the order of 100 a.u. for which any redshift of the emission lines would be almost undetectable.

These results have been shown to apply to other collision systems as well, by explicitly considering Ne^{10+}, P^{15+}, Ar^{18+}, and Kr^{36+}, highlighting, in this sense, the generality of the presented results.

Experimental efforts are needed at this point to further investigate the strong sensitivity of the emission lines described in this work, as well as to establish the potential relevance for astrophysical and laser fusion studies.

ACKNOWLEDGMENTS

Work at Universidad Nacional del Sur is supported by Grants No. PGI 24/F059 and No. PIP 112-201101-00749 of CONICET (Argentina). The authors would like to thank Professor Ron Olson for critically reading this manuscript.

[1] *PENELOPE-2011: A Code System for Monte Carlo Simulation of Electron and Photon Transport*, Workshop Proceedings, edited by F. Salvat, J. M. Fernández-Varea, and J. Sempau (Nuclear Energy Agency OECD, Barcelona, 2011).
[2] G. Y. Liang, F. Li, F. L. Wang, Y. Wu, J. Y. Zhong, and G. Zhao, Astron. J. **783**, 124 (2014).
[3] R. C. Isler, Plasma Phys. Control. Fusion **36**, 171 (1994).
[4] R. Hoekstra, H. Anderson, F. W. Bliek, M. von Hellermann, C. F. Maggi, R. E. Olson, and H. P. Summers, Plasma Phys. Control. Fusion **40**, 1541 (1998).
[5] D. Salzman, *Atomic Physics in Hot Plasmas* (Oxford University Press, Oxford, 1998).
[6] M. S. Murillo, AIP Conf. Proc. **381**, 231 (1996).
[7] M. S. Murillo and J. C. Weisheit, Phys. Rep. **302**, 1 (1998).
[8] H. Zhang, J. G. Wang, B. He, Y. B. Qiu, and R. K. Janev, Phys. Plasmas **14**, 053505 (2007).
[9] L. Zhang, X. Zhao, J. Wan, G. Xiao, W. Duan, X. Qi, and L. Yang, Phys. Plasmas **21**, 093302 (2014).
[10] S. L. Zeng, L. Liu, J. G. Wang, and R. K. Janev, J. Phys. B **41**, 135202 (2008).
[11] L. Liu, J. G. Wang, and R. K. Janev, Phys. Rev. A **77**, 032709 (2008).
[12] L. Liu, J. G. Wang, and R. K. Janev, Phys. Rev. A **79**, 052702 (2009).
[13] D. Jakimovski, L. Liu, J. G. Wang, and R. K. Janev, J. Phys. B **43**, 165202 (2010).
[14] St. Böddeker, S. Günter, A. Könies, L. Hitzschke, and H.-J. Kunze, Phys. Rev. E **47**, 2785 (1993).
[15] R. Abrines and I. C. Percival, Proc. Phys. Soc. London **88**, 873 (1966).
[16] R. E. Olson and A. Salop, Phys. Rev. A **16**, 531 (1977).
[17] R. E. Olson, Phys. Rev. A **24**, 1726 (1981).
[18] R. E. Olson, in *Handbook of Atomic, Molecular, and Optical Processes*, edited by G. Drake (Springer, New York, 2006), Chap. 58.
[19] D. J. W. Hardie and R. E. Olson, J. Phys. B **16**, 1983 (1983).
[20] N. D. Cariatore, S. Otranto, and R. E. Olson, Phys. Rev. A **91**, 042709 (2015).
[21] F. Salvat, J. M. Fernández-Varea, and W. Williamson, Jr., Comput. Phys. Commun. **90**, 151 (1995).
[22] A. I. Akhiezer, I. A. Akhiezer, R. V. Polovin, A. G. Sitenko, and K. N. Stepanov, *Plasma Electrodynamics* (Pergamon, Oxford, 1975), Vol. 2.
[23] Y.-D. Jung, Phys. Plasmas **4**, 21 (1997).
[24] Y.-D. Jung, Phys. Plasmas **5**, 536 (1998).
[25] C.-G. Kim and Y.-D. Jung, Phys. Plasmas **5**, 3493 (1998).
[26] S. Otranto, I. Blank, R. E. Olson, and R. Hoekstra, J. Phys. B **45**, 175201 (2012).
[27] I. Blank, S. Otranto, C. Meinema, R. E. Olson, and R. Hoekstra, Phys. Rev. A **87**, 032712 (2013).